


Synthesis, mechanical properties and iron surface conservation behavior of UV-curable waterborne polyurethane-acrylate coating modified with inorganic carbonate

Jicheng Xu^{1,2} · Yan Jiang¹ · Fengxian Qiu²  · Yuting Dai² · Dongya Yang² · Zongping Yu³ · Pengfei Yang³

Received: 19 July 2017 / Revised: 9 January 2018 / Accepted: 13 February 2018 /
Published online: 17 February 2018
© Springer-Verlag GmbH Germany, part of Springer Nature 2018

Abstract The performances of UV-curable waterborne polyurethane-acrylate (WPUA) composite modified with nano calcium carbonate (NCA) were highlighted in this work. The γ -methacryloxy propyl trimethoxyl silane (KH-570) and polysorbate 80 (Tween-80) were used to enhance interfacial interaction between NCA and WPUA matrix. Transmission electron microscopy (TEM), particle size analysis and Fourier transfer infrared (FT-IR) spectrometry were employed to examine the micromorphology and the variation of function group of modified nano calcium carbonate (MNCA). Three different WPUA oligomers were investigated to obtain the optimized *R* value (the molar ratio of –NCO:–OH) via in situ polymerization and anion self-emulsification process. Results showed that WPUA displayed excellent film-forming ability and mechanical properties when *R* value was 2.2:1.0. These UV-curable WPUA films modified with MNCA (UV-MNCA/WPUA) were prepared through environmentally friendly UV-curable technology and investigated by thermogravimetric (TG) analysis, scanning electron microscope (SEM), X-ray diffractometer (XRD) and FT-IR. UV-MNCA/WPUA-3-3 film had the best overall performances with MNCA-2 and UV-WPUA at the mass ratio of 3.6%. Finally, the experimental results demonstrated that the as-obtained UV-curable coating had outstanding conservation effect to iron surface, providing a promising way for protection of iron cultural relics.

Keywords UV-curable · Calcium carbonate · Waterborne polyurethane-acrylate · Contact angle · Mechanical property

✉ Fengxian Qiu
fxqiu@ujs.edu.cn

¹ Zhenjiang Key Laboratory of Functional Chemistry, Institute of Medicine and Chemical Engineering, Zhenjiang College, Zhenjiang 212003, China

² School of Chemistry and Chemical Engineering, Jiangsu University, Zhenjiang 212013, China

³ Suzhou Mingda Macromolecule Science and Technology CO., Ltd., Suzhou 215234, China

Introduction

Recently, waterborne coating as a new environmentally friendly material has gained widespread concern [1]. UV-curable waterborne technology is a merging method which could combine advantages and overcome drawbacks of waterborne and UV-curable systems [2]. Polyacrylate (PA) possesses remarkable properties in mechanical strength, gloss and resistance to environmental changes [3, 4]. To improve the properties of waterborne polyurethane (WPU), the waterborne polyurethane-acrylate (WPUA) was synthesized and it exhibited outstanding advantages in water resistance, film-forming capability and mechanical properties. Compared with the heat curing and solvent-based coating, UV-curable waterborne polyurethane-acrylate (UV-WPUA) could readily cure. Hence, it is expected to be a promising industrial coating [5].

The development of organic–inorganic nanocomposite is an effective means to obtain new materials [6]. Compared with pure organic polymers, the introduction of inorganic nanocomposites could endow polymer-based nanocomposites many advantages especially in mechanical properties [7]. The morphology, polymorph, particle size and chemical purity are the vital parameters evaluating the organic–inorganic nanocomposites [8]. UV-curable nanocomposites incorporate the properties of nano and UV-curable materials, thus providing the possibility in real application [9, 10].

Calcium carbonate, a commonly used chemical, is considered to be non-toxic and cost-effective in lab-scale research and real application. In addition, it could be prepared with controlled structure and properties applied in organic–inorganic hybrid composites [11]. According to previous studies, calcium carbonate was used in many industries [12] especially in coating, food and ink industries [13, 14]. Besides, calcium carbonate has gained attention in the polyurethane industry because of its flexibility, and hardness [15, 16]. However, calcium carbonate is hard to disperse evenly in organic polymer due to its high specific surface area. Therefore, it limits its application in coatings unless conglomeration is eliminated. Silane coupling agents have been widely applied in various fillers and matrixes, and primers for bonding different materials [17]. It can connect inorganic nanoparticles and organic molecules via the covalent bond [18, 19]. Further, there is little information about the relationship between calcium carbonate content and hybrid composites properties.

There exist irreversibility and the uncertainty in conservation of iron relics. However, there are many materials that could be used in protection of iron relics. The waterborne polyurethane acrylate is an important protection material because of its excellent erosion resistance, lower viscosity and surface tension, strong adhesion and good transparent. In this study, a series of UV-curable MNCA/WPUA (UV-MNCA/WPUA) emulsions were synthesized and used to treat iron substrate, which subsequently investigated in terms of use as protective coatings. NCA was modified with γ -methacryloxy propyl trimethoxyl silane (KH-570) as modifier, and polysorbate 80 (Tween-80) as dispersant. WPU oligomer was prepared using isophorone diisocyanate (IPDI), dimethylolbutanoic acid (DMBA), polyether polyol (NJ-330)

and hydroxyethyl methyl acrylate (HEMA) as raw materials. The best R value and the mass ratio of WPUA: BA: Darocur 1173 were obtained. The effects of the MNCA-2 content on physical, thermal and mechanical properties of the UV-MNCA/WPUA films were also analyzed.

Experimental

Materials

Polyether polyols (NJ-330, $M_n = 3000$ g/mol) was product of Ningwu Chemical CO., Ltd., (Jiangsu, China). Isophorone diisocyanate (IPDI) was obtained from Rongrong Chemical Ltd., (Shanghai, China). Nano calcium carbonate (NCA) was furnished by Guang Yuan Chemical Industry CO., Ltd., (Jiangxi, China). Hydroxyethyl methyl acrylate (HEMA) was purchased from Ruipu New Material Co., Ltd., (Jiangsu, China). Darocur 1173 was provided by Mingda Technology CO., Ltd., (Jiangsu, China). Dimethylolbutanoic acid (DMBA), butyl acrylate (BA), γ -methacryloxy propyl trimethoxyl silane (KH-570), dibutylbis (lauroyloxy) tin (DBTL), polysorbate 80 (Tween-80), triethylamine (TEA), ethanol, and N-methyl-2-pyrrolidone (NMP) were all reagents of Sinopharm Chemical Reagent Co., Ltd., (Shanghai, China).

The surface modification of nano calcium carbonate

Prior to the modification experiment, the original NCA particles were dried at 110 °C in a vacuum oven for 24 h. KH-570 (1 g, 10.0 wt% of NCA) was dissolved in ethanol (50 g) as modifier. Then, Tween-80 (0.1 g, 1.0 wt% of NCA) as dispersant and NCA (10 g) were added into the above solution and dispersed by ultrasonic for 1 h to make KH-570 grafted on the surface of the NCA. The above sample was purified by centrifugal separation and washed with ethanol for three times to remove excessive coupling agent and dispersing agent. Then, the modified nano calcium carbonate (MNCA-2) was obtained after dried under vacuum at 80 °C for 2 h. The resulting powder was ground in an agate mortar and used in the subsequent studies. According to the above methods, modified nano calcium carbonate (MNCA-1) in the absence of Tween-80 was also prepared.

Preparation of WPUA oligomer

A certain amount of IPDI and NJ-330 was mixed into a 250 mL, four-necked, round-bottomed flask equipped with a reflux condenser and mechanical stirrer. Then, two drops of DBTL were added as catalyst at 60 °C for 2 h to obtain –NCO-terminated prepolymer. Then, the prepolymer above was reacted with a certain amount of DMBA (dissolved in NMP) at 80 °C for another 2 h. Next, HEMA was added dropwise and the mixture was reacted consistently at 60 °C for 5 h to form HEMA-capped urethane oligomer. And after that the oligomer capped by HEMA

was stirred and cooled evenly to 40 °C. TEA was added to neutralize the carboxylic acid groups, and the mixture was dispersed into a certain amount of the deionized water and stirred for 30 min.

In this work, three different WPUA prepolymers were prepared via in situ polymerization and anion self-emulsification process with different R value. The basic recipe for WPUA prepolymer is shown in Table 1. Moreover, R value was calculated via computation the molar ratio of $-NCO$ and $-OH$ groups according to the following formula (1):

$$R = \frac{n_{(-NCO)}}{n_{(-OH)}}, \quad (1)$$

where n is the amount of substance (mol).

Preparation of UV-MNCA/WPUA coating

UV-curable coatings were composed of UV-WPUA (WPUA prepolymer, BA as diluting agent and Darocur 1173 as photoinitiator) and MNCA-2. In this work, three series of UV-MNCA/WPUA coatings were obtained and the basic recipe for UV-MNCA/WPUA coatings is listed in Table 2. MNCA-2 (%) is the mass ratio of MNCA-2 to UV-WPUA.

Preparation of UV-MNCA/WPUA coating film

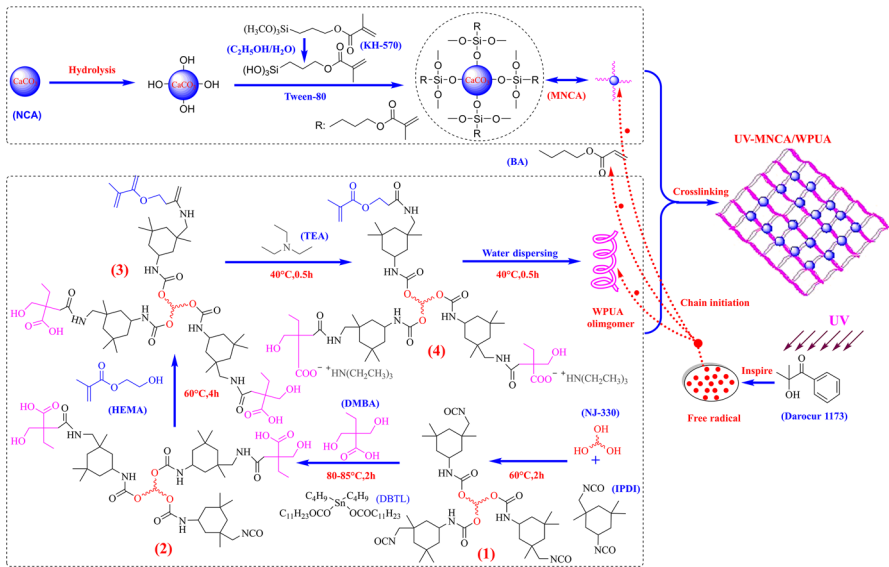
The as-prepared UV-MNCA/WPUA emulsions were casted onto poly (tetrafluoroethylene) boards after ultrasonic dispersion for 0.5 h and dried in a vacuum oven until the emulsion surface was not flow to obtain series of UV-MNCA/WPUA-3 coating films. The films were irradiated by ultraviolet curing machine to activate Darocur 1173, subsequently generating the radicals. The ultraviolet lamp wave length was main 365 nm, and the UV energy was 1000 J/s, the time of exposure to UV irradiation was 30 s, and the distance between the sample and the center of UV lamp was 15 cm. The free radicals could break the double bond in BA, oligomer and MNCA, causing crosslinking. Finally, the UV-MNCA/WPUA films could be prepared. The synthetic route of UV-MNCA/WPUA film is summarized in Scheme 1.

Table 1 The basic recipes for WPUA prepolymer with different R value

Sample	R	IPDI (mmol)	NJ-330 (mmol)	DMBA (mmol)	HEMA (mmol)	TEA (mmol)	NMP (mmol)	Deionized water (mmol)
WPUA-1	2.0:1.0	44.98	6.51	12.76	44.95	12.75	100.88	5000
WPUA-2	2.2:1.0	44.98	5.78	11.81	54.02	11.76	100.88	4833
WPUA-3	2.4:1.0	44.98	5.17	11.00	63.01	10.97	100.88	4722

Table 2 The basic recipes of UV-MNCA/WPUA coatings

Sample	Oligomer	UV-WPUA (100%)			MNCA-2 (%)
		Oligomer (%)	BA (%)	Darocur 1173 (%)	
UV-MNCA/WPUA-1-1	WPUA-1	66	30	4	2.4
UV-MNCA/WPUA-1-2	WPUA-2	66	30	4	2.4
UV-MNCA/WPUA-1-3	WPUA-3	66	30	4	2.4
UV-MNCA/WPUA-2-1	WPUA-2	96	0	4	3.6
UV-MNCA/WPUA-2-2	WPUA-2	86	10	4	3.6
UV-MNCA/WPUA-2-3	WPUA-2	76	20	4	3.6
UV-MNCA/WPUA-2-4	WPUA-2	66	30	4	3.6
UV-MNCA/WPUA-2-5	WPUA-2	56	40	4	3.6
UV- WPUA	WPUA-2	66	30	4	0
UV-MNCA/WPUA-3-1	WPUA-2	66	30	4	1.2
UV-MNCA/WPUA-3-2	WPUA-2	66 <td 30	4	2.4	
UV-MNCA/WPUA-3-3	WPUA-2	66	30	4	3.6
UV-MNCA/WPUA-3-4	WPUA-2	66	30	4	4.8
UV-MNCA/WPUA-3-5	WPUA-2	66	30	4	6.0
UV-MNCA/WPUA-3-6	WPUA-2	66	30	4	7.2



Scheme 1 The synthetic routes of UV-MNCA/WPUA

Characterization and measurements

The distribution of particle diameter and polydispersity (PDI) of emulsions was measured by a high concentration of laser particle size analyzer (BI-9000, USA). The morphology information of the test specimen was observed by transmission electron microscope (FEI Tecnai G² F20 S-TWIN, USA) with an acceleration voltage up to 200 kV. Morphology and composition of the specimens were characterized via a field-emission scanning electron microscope (S-4800, Japan) at an accelerating voltage of 15 kV. The phase of the powers was examined via an X-ray diffractometer (LabX-6000, Japan). FT-IR spectrum of the WPUA prepolymer and UV-MNCA/WPUA specimens were collected via an FT-IR spectrometer (Nexus 670, USA). The apparent viscosity of the WPUA prepolymer was tested by a numerical viscometer (NDJ-9S, China). The hardness was performed on a sclerometer (KYLX-A, China). Tensile strength test and elongation at break testing for the test specimens were performed on a tensile tester (KY-8000A, China) at ambient temperature. The contact angle was tested by a commercial optical system (CAM200, Finland), equipped with a high-speed camera. Thermogravimetric analysis (TGA) and Differential scanning calorimetry (DSC) of UV-curable coating films were performed on a Netzsch instrument (204 F1, Germany).

WPUA prepolymer was poured into a 30 mL container and warmed to 120 °C for 48 h in a temperature-controlled oven. Then, the container was transferred into a desiccator and weighted again after cool. The sample was weighted for several times after heating until constant weight. The solid mass fraction of WPUA oligomer, ω_1 , was calculated according to the following Eq. (2):

$$\omega_1 = \frac{W_2}{W_1} \times 100\%, \quad (2)$$

where W_1 , W_2 is the mass of WPUA prepolymer and container before and after being placed into the oven, respectively.

The films were tailored to a specific shape (3 × 3 cm) and immersed in deionized water (or ethanol) at ambient temperature after being weighted. Then, the films were wiped with a piece of filter paper to remove the water (or ethanol) on the film surface after 24 h and then weighted again. The water absorption (or gel content), ω_2 , was calculated according to the following Eq. (3):

$$\omega_2 = \frac{m_2 - m_1}{m_1} \times 100\%, \quad (3)$$

where m_1 , m_2 is the mass of the film before and after being immersed the water (or ethanol), respectively.

Two thin rectangle (2 × 2.5 cm) tinplate iron sheets were burnished with sand paper. One was covered with UV-MNCA/WPUA-3-3 coating and was irradiated under the UV curing machine for about 30 s to cure coating. The other was untreated sample as comparison. Both iron sheets were exposed to natural environment. After the same days, the surface changes of iron sheets were captured by a digital display camera.

Results and discussion

The effect of modification on NCA

The NCA dispersion is a significant factor in characterizing composite performance. The particle size and PDI of the NCA, MNCA-1 and MNCA-2 are shown in Fig. 1.

As can be seen from Fig. 1, the particle size of NCA and MNCA-1 was about 283 and 268 nm, respectively, whereas that of MNCA-2 was about 250 nm. The particle size of MNCA-1 did not significantly decrease, which is mainly attributed to interaction between the $-OH$ groups from NCA surface with $-Si-OCH_3$ groups from the KH-570 and the increase of steric effect [20]. However, Tween-80 was added into the system as dispersant, causing the particle size decreasing from 283 to 250 nm. This was because Tween-80 could inhibit the coagulation of the particles. In order to further investigate the microtopography and structure of three particles, TEM analysis should be given to provide the further corroboration.

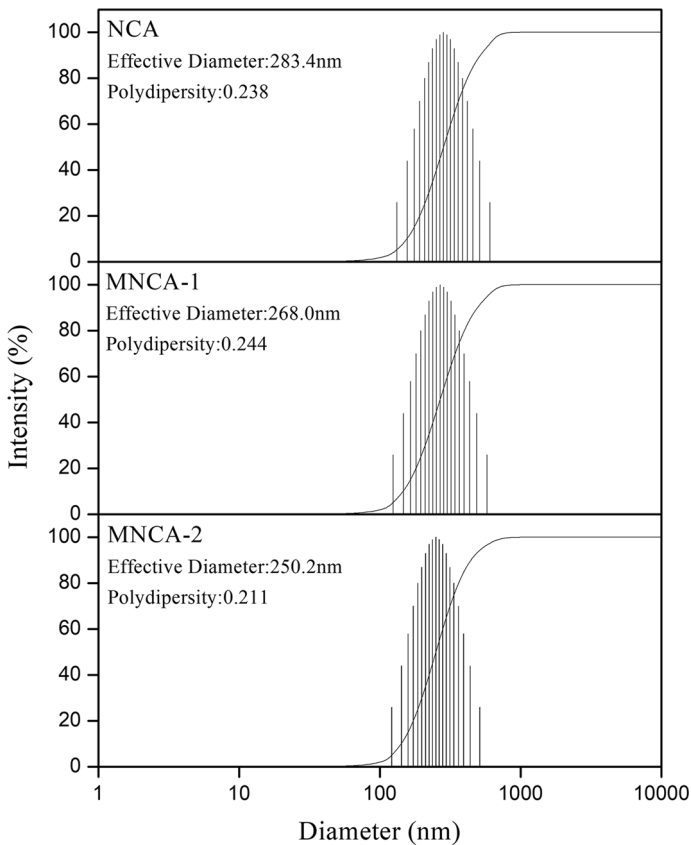


Fig. 1 The particle size and PDI of the NCA, MNCA-1 and MNCA-2

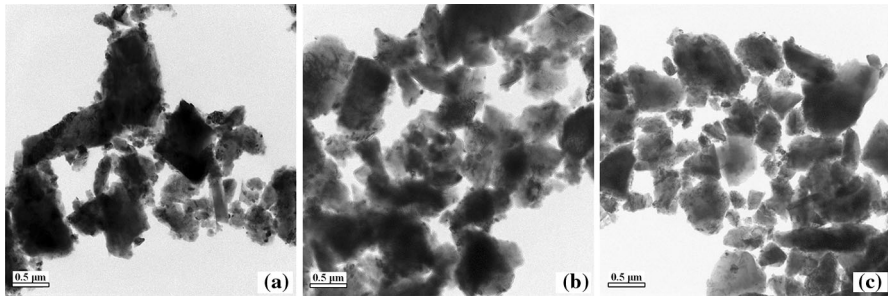


Fig. 2 TEM images of NCA (a), MNCA-1 (b) and MNCA-2 (c)

TEM images of NCA (a), MNCA-1 (b) and MNCA-2 (c) are displayed in Fig. 2. From Fig. 2a and b, NCA particles were gathered together and the dispersion of MNCA-1 particles had a few changes. However, homogeneous dispersion was found in MNCA-2 particles in Fig. 2c. It was mainly because that some organic chains were replaced by the active group of NCA surface, which could result in steric hindrance effect, and thus effectively inhibited NCA particle agglomeration. The molecular of KH-570 connecting with the NCA particles produced mutual exclusion and steric hindrance effect. Moreover, the surface free energy was reduced relatively, thereby reducing the molecular reunion effectively. These results indicated that coupling agents KH-570 and nonionic surfactant Tween-80 could improve NCA dispersion and surface performance effectively.

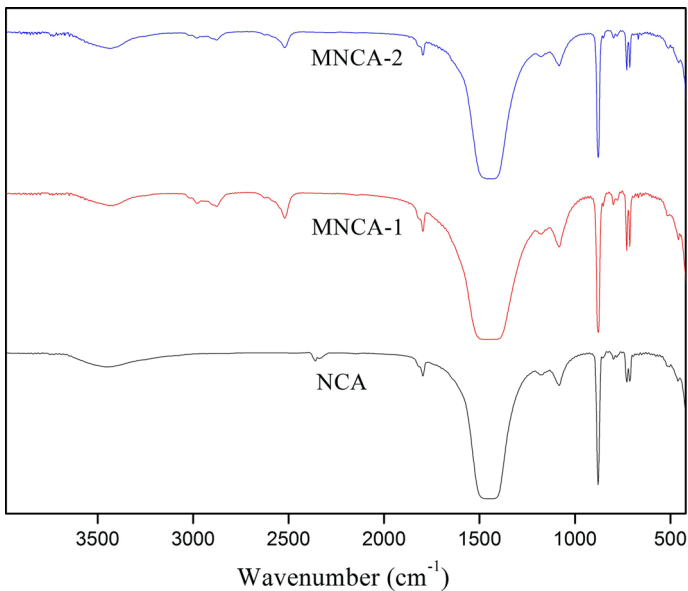


Fig. 3 FT-IR spectra of NCA, MNCA-1 and MNCA-2

FT-IR spectra of NCA, MNCA-1 and MNCA-2 are shown in Fig. 3. The distinct peaks at 1462, 875 and 711 cm^{-1} were corresponded to the feature absorption peaks of NCA. The absorption intensity of carbonate in NCA was enhanced after modification. The C–H stretching vibration absorption peak of alkane and olefin was obviously in the range of 3000–2800 cm^{-1} . Compared with the spectrum of the untreated NCA, the absorption peaks at 2870–2980 cm^{-1} appeared in the spectra of MNCA-1 and MNCA-2, which could be ascribed to the stretching mode of C–H in KH-570. The above result indicated that KH-570 was not physically loaded on NCA particles, but linked together by covalent bonds. The amount of Tween-80 was less so that there was no obvious difference between the FT-IR of MNCA-1 and MNCA-2.

These results confirmed that the KH-570 was grafted on the surface of NCA particles by chemisorption, which were consistent with the particles and TEM analysis. Therefore, the MNCA-2 sample was selected to make subsequent experiments in this work.

The effect of *R* value on the properties of WPUA oligomer and UV-MNCA/WPUA film

The physical properties of WPUA oligomer

Table 3 lists the physical properties of WPUA oligomers. The actual solid content of WPUA-2 oligomer was closest to the design value (27.8%). In Table 3, the apparent viscosities of WPUA oligomers decreased with the increase of *R* value, which was because a low concentration chain extender could lead to a lower molecular weight and less branched chains on the polyurethane backbone chains. Particle size is a key parameter of water polyurethane dispersions, which will affect the performance of water polyurethane in the final industrial applications [21]. Furthermore, the particle size will increase with the increasing viscosity of dispersant, thereby further affecting the prepolymer molecular weight and molecular structure [22]. In Table 3, it could be found that the particle size of WPUA oligomers decreased with *R* value rising, but PDI was opposite, because of the decrease in the hydrophilic –COOH group content in DMBA. PDI represented the dispersion degree of emulsion and PDIs of WPUA oligomers were 0.102, 0.107

Table 3 The physical properties and film-forming ability of WPUA oligomers

Sample	WPUA-1	WPUA-2	WPUA-3
Solid mass fraction (%)	23.34	24.18	22.95
Apparent viscosity (mPa·s)	15.4	8.5	7.1
Particle size (nm)	52.2	45.8	45.0
PDI	0.102	0.107	0.120
Appearance	White	Transparent	Transparent
Stability of emulsion (months)	15	15	15

and 0.120, respectively, indicating that it had a good dispersity [23, 24]. From Table 3, in the case of the emulsion appearance, the WPUA-1 oligomer was presented in a white emulsion and WPUA-2 and WPUA-3 oligomers presented in transparent dispersions. In the case of the emulsion stability, all oligomers were validated over 15 months from the date of manufacturing, showing an excellent stored stability [25].

FT-IR of the WPUA oligomer

The successful polymerization was investigated by FT-IR spectra. FT-IR spectra of WPUA oligomers are shown in Fig. 4. The bands at $3330\text{--}3360\text{ cm}^{-1}$ ($-\text{NH}$), $2855\text{--}2955\text{ cm}^{-1}$ ($-\text{CH}_2$ and $-\text{CH}_3$), 1724 cm^{-1} ($\text{C}=\text{O}$), 1360 cm^{-1} ($\text{C}-\text{N}$) and 1110 cm^{-1} ($\text{C}-\text{O}-\text{C}$) indicated the presence of urethane in WPUA oligomers. It should be pointed out that the peak at 2270 cm^{-1} vanished in all WPUA oligomers spectra, indicating that $-\text{NCO}$ group was reacted with $-\text{OH}$ thoroughly. In addition, the absorption peak at 840 cm^{-1} corresponded to acrylate characteristic peak. Moreover, the presence of the peak at about 1680 cm^{-1} ($\text{C}=\text{C}$ stretching vibration from the $\text{C}=\text{C}$ stretching vibration) in all samples demonstrated that oligomers were composed of polyurethane and acrylate.

The film-forming ability of UV-MNCA/WPUA-1

To compare the appearance of different films, the surface pictures of UV-MNCA/WPUA-1-1 (a), UV-MNCA/WPUA-1-2 (b) and UV-MNCA/WPUA-1-3 (c) films are shown in Fig. 5. From Fig. 5a and b, UV-MNCA/WPUA-1-1 and UV-MNCA/

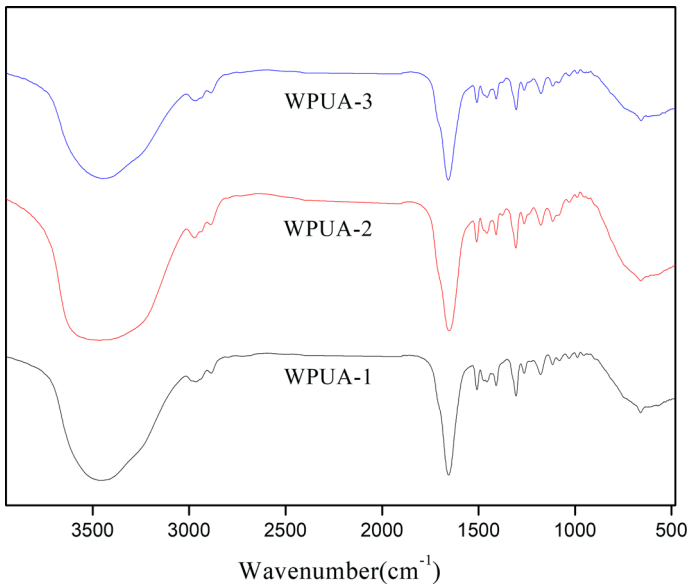


Fig. 4 FT-IR spectra of the WPUA oligomers

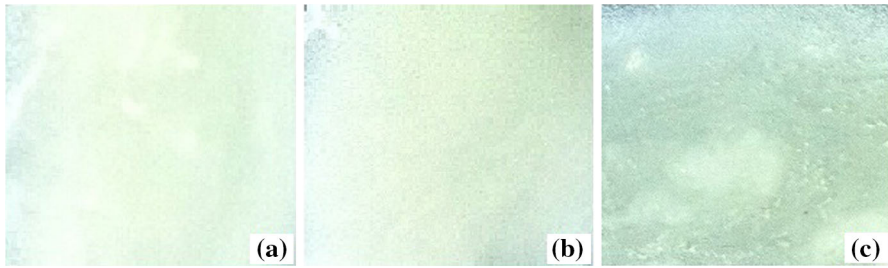


Fig. 5 The surface pictures of UV-MNCA/WPUA-1-1 (a), UV-MNCA/WPUA-1-2 (b) and UV-MNCA/WPUA-1-3 (c) films

WPUA-1-2 films were smooth and well distributed. However, the particles of MNCA-2 in UV-MNCA/WPUA-1-3 film (Fig. 5c) were conglomeration, causing the film surface uneven and irregular. These results implied that UV-MNCA/WPUA-1-1 and UV-MNCA/WPUA-1-2 samples had a good film forming property under UV irradiation.

The water absorption (or gel content) and mechanical properties of UV-MNCA/WPUA-1 series films

Compared with solvent-based materials, the waterproof of WPUA films, as one of the major drawbacks, has attracted extensive attention. The water absorption was utilized to investigate the water resistance of the coating films. The water absorption or gel content of series of UV-MNCA/WPUA-1 films was examined and the corresponding results are summarized in Table 4. The water absorption (or gel content) of the UV-MNCA/WPUA-1 film reduced with R valve rising, indicating water resistance increased. Tension tests were performed to study the essential mechanical properties of the modulus, elongation at break, maximum tensile strength and toughness of the polymeric materials [26]. The tensile strength of UV-MNCA/WPUA-1-2 was 8.60 MPa, which was higher than others, indicating that UV-MNCA/WPUA-1-2 provided a better crosslinking structure. Series of UV-MNCA/WPUA-1 samples had an identical soft and hard block, while the value of R was different, so the contents of ionic groups were also different. The hard

Table 4 The water absorption and mechanical properties for series of UV-MNCA/WPUA-1 films

Sample	UV-MNCA/WPUA-1-1	UV-MNCA/WPUA-1-2	UV-MNCA/WPUA-1-3
Water absorption (%)	8.56	5.17	4.28
Gel content (ethanol, %)	143.17	97.50	84.64
Hardness (shore A)	89.1 ± 0.1	91.6 ± 0.2	92.8 ± 0.2
Tensile strength (MPa)	1.43	8.60	3.58
Elongation at break (%)	275.77	165.84	106.22

segment increased with R value increase, so the hardness of series of UV-MNCA/WPUA-1 films increased slowly.

The above results confirmed that the WPUA-2 had optimal comprehensive performance and was chosen for the further study in this paper ($R = 2.2:1.0$).

Effect of BA content on the mechanical properties of UV-MNCA/WPUA

Series of UV-MNCA/WPUA-2 coatings were obtained with different mass ratio of oligomer: BA: Darocur 1173 when the mass ratio of MNCA-2 to UV-WPUA was 3.6%. Figure 6 presents the effect of the BA content on the strain–stress behavior (a), the maximum tensile strength and elongation at break (b). The results indicated that UV-MNCA/WPUA-2-4 composite had optimum mechanical properties. It was found that the tensile strength and elongation at break increased with the mass ratio of BA increase except UV-MNCA/WPUA-2-5 film, which was mainly caused by the presence of the crosslinking network structure between PU, PA and intermolecular hydrogen bonds. The special flexible acrylic resin molecular chain segment made both the tensile strength and elongation increase. The results demonstrated that the as-prepared films had excellent mechanical properties and elongation at break. In UV-MNCA/WPUA-2-5, WPUA content was too low to react completely with BA and MNCA-2 under UV light, causing the tensile strength or elongation at break to decrease. Similarly, the elongation at break increased with BA content rising at first, which was responsible for the deformation mechanism of WPUA. WPUA possessed soft and hard block structure, the hard segments of which could be tilted towards the stretching direction at low strain. Conversely, they aligned parallel to the stretching direction in the high strain [27]. In this study, series of UV-MNCA/WPUA-2 films could resist higher stress because of the introduction of BA.

Moreover, UV-MNCA/WPUA-2-4 showed the highest initial modulus and tensile strength as well as elongation at break, which could be attributed to a closely crosslink structure and a higher conversion rate. Therefore, the mass ratio of oligomer: BA: Darocur 1173 was selected 66%:30%:4% to further study.

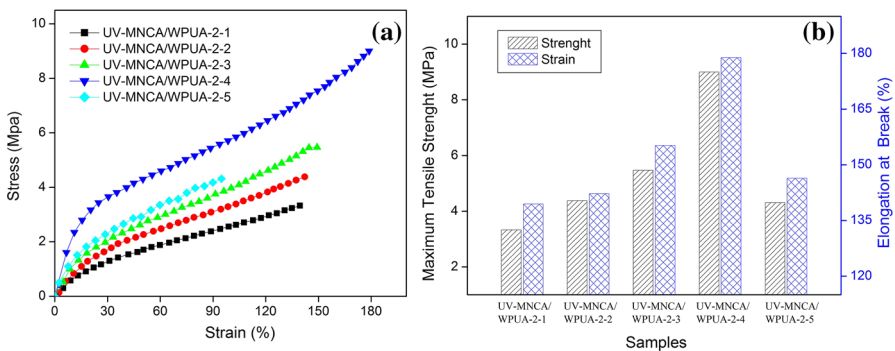


Fig. 6 Tensile behavior of the UV-MNCA/WPUA-2 series films: **a** strain–stress curves, **b** maximum tensile strength and elongation at break

The effect of MNCA-2 content on UV-MNCA/WPUA film

In order to understand the effect of MNCA-2 content on UV-MNCA/WPUA films, water absorption, gel content, contact angle, hardness and mechanical properties of all samples were tested and the corresponding results are listed in Table 5.

Effect of MNCA-2 content on the water absorption and gel content of UV-WPUA and UV-MNCA/WPUA-3 series films

Effect of MNCA-2 content on the water absorption and gel content of UV-MNCA/WPUA film is listed in Table 5. Compared with the pure UV-WPUA film, the water absorption of series of UV-MNCA/WPUA-3 films decreased from 9.35 to 4.27% at a low concentration of MNCA-2 ($\leq 3.6\%$). The water resistant of the UV-WPUA films had been enhanced because of the formation of hydrogen bonding between the hydroxyl group of MNCA-2 and the carboxyl group or amine group of WPUA. UV-MNCA/WPUA-3 films possessed the compact structures due to physical crosslinking among the WPUA, BA and MNCA-2 particles; thus, the water absorption of UV-MNCA/WPUA-3 films decreased. However, the water absorption of films increased in excessive the MNCA-2 content ($> 3.6\%$), which was caused by much stronger polar MNCA-2 particles enriched on the films surface.

Effect of MNCA-2 content on the contact angle analysis of UV-WPUA and UV-MNCA/WPUA-3 series films

According to the data in Table 5, it could be found that the contact angles of UV-WPUA and UV-MNCA/WPUA-3 films increased from 64.28° to 82.38° . Compared with UV-WPUA film, the contact angles of UV-MNCA/WPUA-3 films were relatively higher, illustrating that the interfusion of MNCA-2 had positive effects on the water resistance. With the increasing MNCA-2 content, the contact angle of UV-MNCA/WPUA-3 increased initially and then decreased. The results also indicated that MNCA-2 could improve the water resistance of UV-WPUA film.

Effect of MNCA-2 content on the mechanical properties of UV-WPUA and UV-MNCA/WPUA-3 series films

The hardness is related to the mechanical behaviors and toughness of the films. Table 5 shows the hardness of UV-WPUA and UV-MNCA/WPUA-3 series films. Compared with the pure UV-WPUA film, the hardness of UV-MNCA/WPUA-3 series films increased from 82.5 to 93.3 with the MNCA-2 content increase, showing that the addition of MNCA-2 had a pronounced positive effect on the hardness of films.

Strain–stress curves of UV-WPUA and UV-MNCA/WPUA-3 films are presented in Fig. 7. Furthermore, the detailed data of tensile strength and elongation at break are shown in Table 5. Figure 7 shows that the introduction of the MNCA-2 could significantly enhance the tensile strength because of the strong interactions between the WPUA matrix and MNCA-2 nanoparticles. It was also found that the tensile

Table 5 The properties of UV-MNCA/WPUA-3 series films

Sample	UV-MNCA/WPUA-3					
	1	2	3	4	5	6
Water absorption (%)	6.24	5.17	4.27	6.53	7.48	8.66
Gel content (%)	98.98	97.5	79.75	77.39	75.09	72.87
Contact angle (°)	64.28	73.13	82.38	79.24	74.31	72.13
Hardness (shore A)	82.5 ± 0.3	91.6 ± 0.2	92.2 ± 0.1	92.6 ± 0.2	93.0 ± 0.3	93.3 ± 0.2
Tensile strength (MPa)	5.63	8.60	9.00	8.22	7.51	6.76
Elongation at break (%)	122.14	195.84	178.89	178.54	143.25	165.05
T_d max (°C)	458.3	719.1	721.7	723.1	725.9	727.3

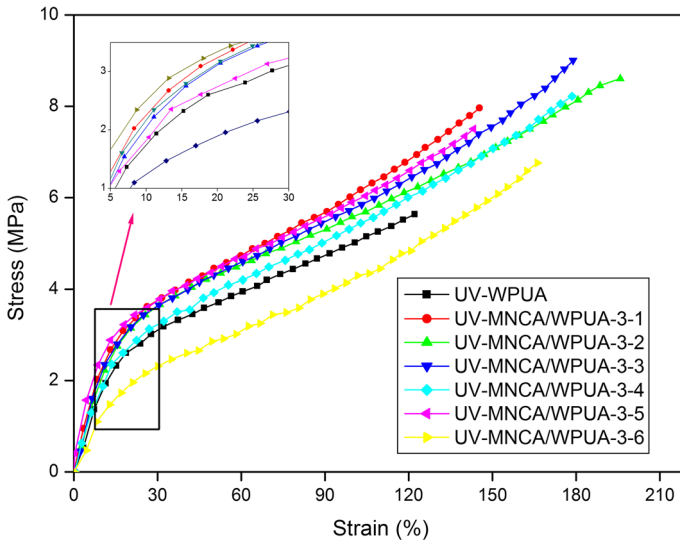


Fig. 7 Strain-stress curves of UV-WPUA and UV-MNCA/WPUA-3 series films

strength of all the UV-MNCA/WPUA-3 series films was higher than that of UV-WPUA film, which was most likely because crosslinking density increased with the addition of the MNCA-2 and BA, promoting the tensile strength of films. On the other side, the enhancement in the tensile strength indicated that strong interfacial interactions existed in among the MNCA-2 surface, BA and the nearby WPUA chains. In Fig. 7, when the MNCA-2 content was the mass ratio of 3.6%, the tensile strength was the highest. When the MNCA-2 content was more than mass ratio of 3.6%, the tensile strength decreased, caused by the incompatibility between the MNCA-2 and the WPUA matrix under UV irradiation.

The FT-IR of the UV-curable coating films

The UV-WPUA and part of UV-MNCA/WPUA-3 series films were characterized by FT-IR spectra, and the characteristic absorbance peaks of UV-WPUA and UV-MNCA/WPUA-3 series films could be observed in Fig. 8. The absorption peaks at $3400\text{--}3600\text{ cm}^{-1}$ were assigned to --NH and --OH stretching vibrations. The peak at 1110 cm^{-1} was corresponding to the characteristic peak of C--O--C groups. The peak around $1700\text{--}1730\text{ cm}^{-1}$ could be ascribed to the absorption peak of C=O groups. In addition, the characteristic peak around $2972\text{--}2868\text{ cm}^{-1}$ was attributed to the asymmetric and symmetric stretching vibration of C--H in hydrogen bonding. Compared with the spectrum of UV-WPUA sample, the representative functional groups in the spectra of UV-MNCA/WPUA-3 series films were consistent, indicating that the structure of WPUA was unaffected after the addition of MNCA-2. Hence, the above results indicated that there were no obvious chemical structural changes in UV-WPUA materials after the introduction of MNCA-2 [28].

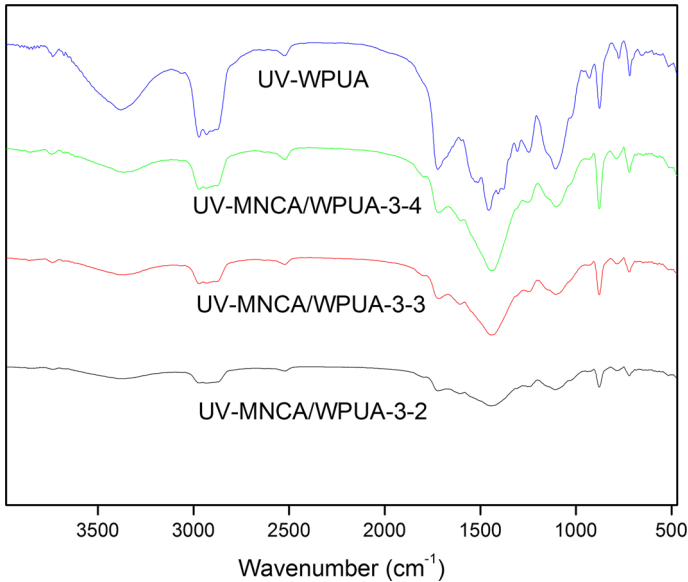


Fig. 8 FT-IR spectra of UV-WPUA and UV-MNCA/WPUA-3 series films

Thermal properties of UV-WPUA film

The thermal properties of the UV-WPUA films containing different MNCA-2 content were evaluated by the TGA. Generally, the thermal stability of UV-WPUA was affected by the number of the secondary interactions (such as hydrogen bonding) and urethane linkages in their matrix, as they could improve the tolerance towards a considerable amount of heat. In addition, the interfusion of MNCA-2 particles also was conducive to improve the thermal stability of the UV-WPUA films.

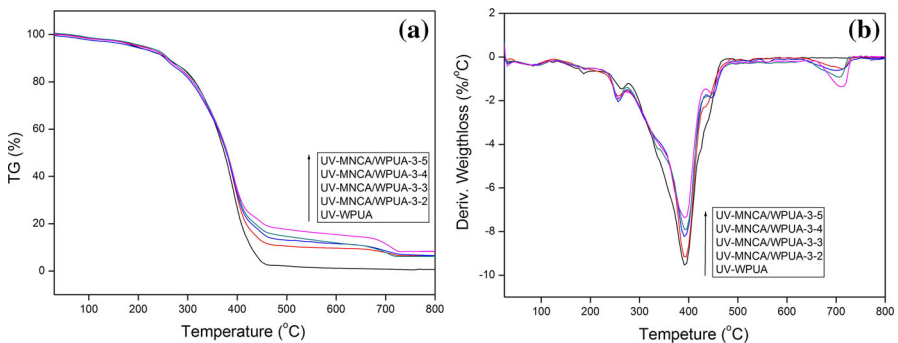


Fig. 9 TG (a) and DTG (b) curves of UV-WPUA, UV-MNCA/WPUA-3-2, UV-MNCA/WPUA-3-3, UV-MNCA/WPUA-3-4 and UV-MNCA/WPUA-3-5 films

TG (a) and DTG (b) curves of UV-WPUA, UV-MNCA/WPUA-3 series films are presented in Fig. 9. Normally, the thermal decomposition of WPUA could be divided into two stages: the first stage was the hard segment undergoes decomposition reaction of polyurethane. The consequent stage was dominated by the isocyanates and polyol decomposition, which was influenced by the soft segment content. It was generally known that thermal decomposition temperature of the material was consistent with the temperature at the maximum mass loss rate in TG curves. As can be seen from Fig. 9a, compared with the UV-WPUA film, the initial decomposition temperature of UV-MNCA-WPUA-3 series films increased from 230 to 250 °C with the introduction of MNCA-2, which might be caused by the rise of intermolecular attractions, such as hydrogen bonding, polar–polar interaction between MNCA-2, BA and WPUA matrix. The second decomposition temperature increased about 5 °C after the introduction of MNCA-2. The residual content of UV-MNCA/WPUA composite at 490 °C was higher than that of pure UV-WPUA composite. The residual amount of the composite around 500 °C was in accordance with the additional amount of MNCA-2. Figure 9b shows DTG thermal curves of the films, in which the main decomposition peak of carbonate to CO₂ was found at 715 °C. These results indicated that compared with pure UV-WPUA, UV-MNCA/WPUA-3 series films achieved a higher thermal stability, which was mainly thanks to the strong force between MNCA-2 and WPUA matrix under UV irradiation. Hence, the introduction of MNCA-2 could dramatically improve the thermal properties of UV-WPUA, which could be attributed to the great dispersion of inorganic filler in UV-WPUA.

In Fig. 9a, a significant weight loss was also found at UV-WPUA sample. The weight reductions were due to the decomposition of WPUA polymers around 230–490 °C. Figure 9b shows more pronounced endothermic peak around 390 °C. Moreover, an unapparent weight loss could be observed at temperature range of 660–740 °C, with a corresponding indistinct endothermic peak at about 715 °C, which could be ascribed to the decomposition of CaCO₃ to CaO [29]. The remaining mass of UV-WPUA, UV-MNCA/WPUA-3-2, UV-MNCA/WPUA-3-3, UV-MNCA/WPUA-3-4 and UV-MNCA/WPUA-3-5 is 2.08, 9.75, 11.58, 25.06 and 29.46%, respectively. In addition, $T_{d \max}$ data are listed in Table 5, showing that the temperature increased from 458.3 to 727.3 °C.

The DSC analysis results of UV-WPUA and UV-MNCA/WPUA-3 series films are presented in Fig. 10. Firstly, the exothermic peak was observed at around 200 °C and the endothermic peak was discovered at around 270 °C for all curves, which might be a tiny bit of water from the composite surface or chemical reaction. The relatively exothermic peak beginning at 230 °C came from the decomposition of WPUA. The decalescence peaks in the DSC curves (except UV-WPUA) were found around 715 °C, indicating that MNCA-2 began decomposing in this period.

SEM analysis

The cross-section morphology of UV-WPUA film (a) and UV-MNCA/WPUA-3-3 film (b) was investigated by SEM. From Fig. 11a, the cross-section of the pure UV-WPUA was smooth, while that of UV-MNCA/WPUA-3-3 (Fig. 11b) was rough and

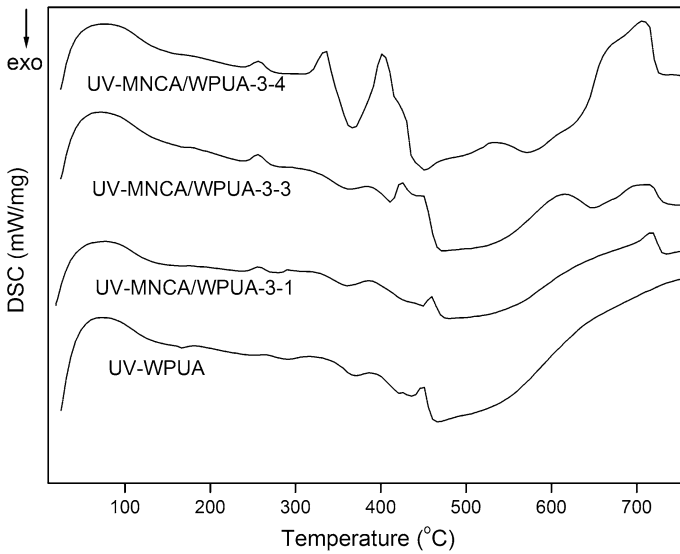


Fig. 10 DSC curves of UV-WPUA and UV-MNCA/WPUA-3 series films

uneven, caused by MNCA-2 particles. Moreover, significant changes in cracks or phase separation in the UV-WPUA surface were not observed, illustrating that UV-WPUA film had a good microstructure. Figure 11b shows that silane coupling agent facilitated the dispersion properties of the NCA and, thus, MNCA-2 particles were wrapped by WPUA oligomer and dispersed evenly on the surface, which could be attributed to the chemical reaction between KH-570, WPUA oligomer and BA. Finally, most MNCA-2 particles were fractured and only a few MNCA-2 are pulled out from WPUA matrix, demonstrating that all WPUA oligomers reacted with MNCA-2 completely under UV irradiation.

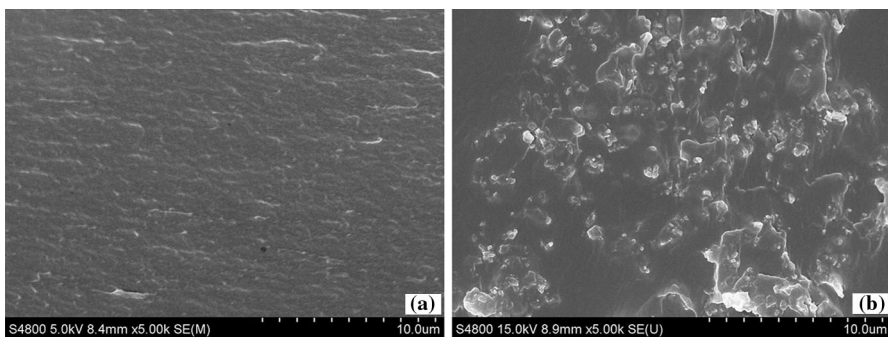


Fig. 11 SEM images of UV-WPUA (a) and UV-MNCA/WPUA-3-3 (b)

XRD analysis

The higher the intensity of the diffraction peaks, the higher the crystallinity in the polyurethane. XRD patterns of MNCA-2, UV-MNCA/WPUA-3-3 and UV-WPUA films are shown in Fig. 12. In MNCA-2, the peaks at $2\theta = 29.4^\circ$, 31.52° , 39.4° , 43.19° , 47.51° and 48.52° could be indexed as the typical phase of (104), (006), (113), (202), (018) and (116) of CaCO_3 (JCPDS 88-1808). In Fig. 12, a diffused diffraction peak around 20° was discovered at the UV-WPUA and UV-MNCA/WPUA-3-3 coating XRD patterns, which could be put down to the short-range-order arrangement of chain segments of amorphous polyurethane in WPUA and the formation of a uniform three-dimensional reticulation structure interspersed with the WPUA segment [30]. All peaks of MNCA-2 were observed in XRD patterns of UV-MNCA/WPUA-3-3 film, indicating that MNCA-2 was successfully incorporated and it did not change the original structure of polyurethane. These results further confirmed that there existed strong interaction between WPUA and CaCO_3 nanoparticles.

Application of UV-MNCA/WPUA coating

These excellent properties indicated that as-prepared UV-MNCA/WPUA has a great potential application and the UV-MNCA/WPUA-3-3 coating was selected for the further iron protection application study. The naked iron and the treated iron samples were placed in natural environment for several days to evaluate the conservation performance of UV-MNCA/WPUA-3-3 emulsion. The images of iron

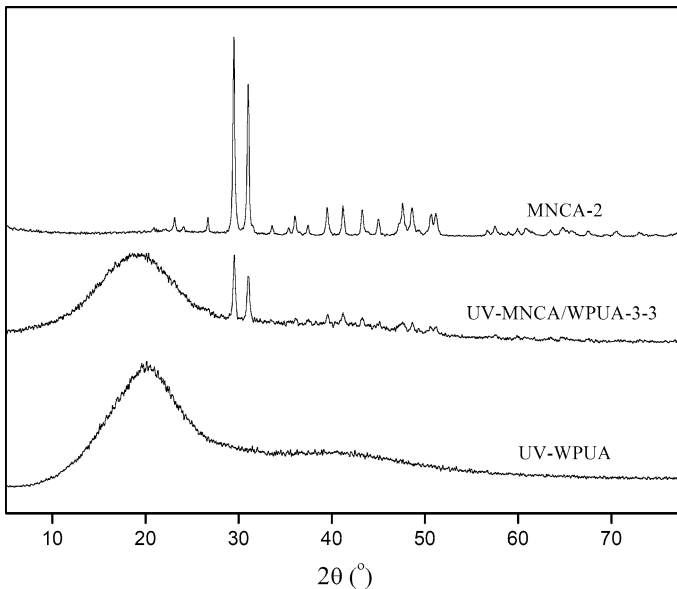


Fig. 12 XRD patterns of MNCA-2, UV-MNCA/WPUA-3-3 and UV-WPUA films

sheet treated with UV-MNCA/WPUA-3-3 coating and naked iron are displayed in Fig. 13. Their physical appearance was scrutinized and the corrosive behaviors were carefully observed. As can be seen from Fig. 13, 5 days later, the blank iron sheet started rusting and became more and more serious after long-term exposure to natural environment. However, after 21 days, the iron sheet covered with UV-MNCA/WPUA-3-3 coating had no obvious change under the same conditions. The results showed that the as-prepared UV-MNCA/WPUA-3-3 coating played a very good protection to iron material.

Conclusions

The nano calcium carbonate was successfully modified with KH-570 and Tween 80, which was confirmed by particle size test, FT-IR spectra and TEM images. Compared with NCA, the MNCA-2 reduced agglomerations at certain degree, which had a smaller particle size and integrated closely with WPUA oligomer through chemical bonds. A series of WPUA oligomers were acquired via the reaction with IPDI, NJ-330, DMBA and HEMA with in situ and anionic self-emulsifying method. By the analyses of film-forming ability, water absorption and mechanical properties, the optimal *R* value was selected as 2.2:1.0. A series of UV-MNCA/WPUA composite films were prepared by MNCA-2, BA and WPUA and characterized by contact angle, FT-IR, XRD and SEM. When the mass ratio of oligomer: BA: Darocur 1173 was 66%:30%:4%, the film had the best mechanical properties. The FT-IR spectra showed that there was no obvious influence on the chemical structural of WPUA with the addition of MNCA-2. The addition of MNCA-2 could also bring a synchronous improvement in mechanical and heat-aging properties of UV-WPUA film. Furthermore, when the mass ratio of MNCA-2 to WPUA was 3.6%, UV-MNCA/WPUA-3-3 film had the best mechanical properties and thermal properties. Therefore, UV-MNCA/WPUA-3-3 coating was applied in the protection of iron. The results showed that UV-MNCA/WPUA-3-3 coating could effectively reduce the erosion of external factors.

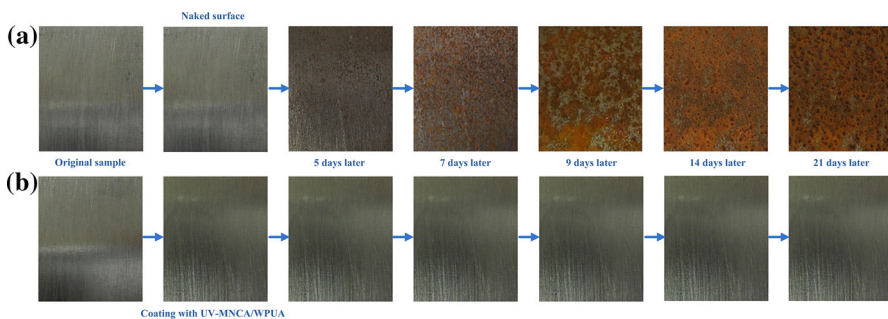


Fig. 13 Images of iron sheet after covered UV-curable coating film and naked surface

Acknowledgements This Project was supported by the Natural Science Foundation of Jiangsu Province (BK20161362 and BK20161264), 333 High-Level Personnel Training Project of Jiangsu Province (BRA2016142) and Zhenjiang College Scientific Research Team (ZJCKYD2017023).

References

1. Lin XF, Zhang SY, Qian J (2014) Synthesis and properties of a novel UV-curable waterborne hyperbranched polyurethane. *J Coat Technol Res* 11:319–328
2. Xu JC, Rong XS, Chi TY, Wang M, Wang YY, Yang DY, Qiu FX (2013) Preparation, characterization of UV-curable waterborne polyurethane-acrylate and the application in metal iron surface protection. *J Appl Polym Sci* 130:3142–3152
3. Chen Q, Wen WY, Qiu FX, Xu JC, Yu HQ, Chen ML, Yang DY (2016) Preparation and application of modified carboxymethyl cellulose Si/polyacrylate protective coating material for paper relics. *Chem Pap* 70:946–959
4. Zhang XY, Wen WY, Yu HQ, Chen Q, Xu JC, Yang DY, Qiu FX (2016) Preparation and artificial ageing tests in stone conservation of fluorosilicone vinyl acetate/acrylic/epoxy polymers. *Chem Pap* 70:1621–1631
5. Xu HP, Qiu FX, Wang YY, Wu WL, Yang DY, Guo Q (2012) UV-curable waterborne polyurethane-acrylate: preparation, characterization and properties. *Prog Org Coat* 73:47–53
6. Yang DY, Zhang HQ, Qiu FX, Han L (2012) Investigation of polyurethane (urea)/modified nano-calcium carbonate hybrid aqueous dispersions and their films. *J Appl Polym Sci* 125:2896–2901
7. Zhao ZP, Guo Q, Qian JZ, Pan GL (2012) Mechanical properties and tribological behaviour of polyurethane elastomer reinforced with CaCO_3 nanoparticles. *Polym Polym Compos* 20:575–580
8. Zhang CX, Zhang JL, Feng XY, Li W, Zhao YL, Han BX (2008) Influence of surfactants on the morphologies of CaCO_3 by carbonation route with compressed CO_2 . *Colloid Surf A* 324:167–170
9. Mohseni M, Bastani S, Jannesari A (2014) Influence of silane structure on curing behavior and surface properties of sol-gel based UV-curable organic-inorganic hybrid coatings. *Prog Org Coat* 77:1191–1199
10. Donate-Robles J, Martín-Martínez JM (2011) Comparative properties of thermoplastic polyurethane adhesive filled with natural or precipitated calcium carbonate. *Macromol Symp* 301:63–72
11. Gao XY, Zhou B, Guo YP, Zhu YC, Chen X, Zheng YH, Gao W, Ma XY, Wang ZC (2010) Synthesis and characterization of well-dispersed polyurethane/ CaCO_3 nanocomposites. *Colloid Surf A* 371:1–7
12. De Sa e Sant’Anna S, De Souza DA, De Araujo DM, Carvalho CD, Yoshida MI (2008) Physico-chemical analysis of flexible polyurethane foams containing commercial calcium carbonate. *Mater Res* 11:433–438
13. Cheng B, Lei M, Yu J, Yu JG, Zhao XJ (2004) Preparation of monodispersed cubic calcium carbonate particles via precipitation reaction. *Mater Lett* 58:1565–1570
14. Donate-Robles J, Martín-Martínez JM (2011) Addition of precipitated calcium carbonate filler to thermoplastic polyurethane adhesives. *Int J Adhes Adhes* 31:795–804
15. Betingyte V, Zukiene K, Jankauskaite V, Milasiene D, Mickuk KV, Gulbiniene A (2012) Influence of calcium carbonate fillers on the properties of recycled poly (ε-caprolactone) based thermoplastic polyurethane. *Mater Sci* 18:243–249
16. Yao L, Yang J, Sun J, Cai LF, He LH, Huang H, Song R, Hao YM (2011) Hard and transparent hybrid polyurethane coatings using in situ incorporation of calcium carbonate nanoparticles. *Mater Chem Phys* 129:523–528
17. Vrsaljko D, Blagojevic SL, Leskovic M, Kovacevic V (2008) Effect of calcium carbonate particle size and surface pretreatment on polyurethane composite part I: interface and mechanical properties. *Mater Res Innov* 12:40–46
18. Bin L, Song-Mei L, Jian-Hua L, Mei Y (2014) The heat resistance of a polyurethane coating filled with modified nano- CaCO_3 . *Appl Surf Sci* 315:241–246
19. Yan XX, Xu GY (2012) Influence of silane coupling agent on corrosion-resistant property in low infrared emissivity Cu/polyurethane coating. *Prog Org Coat* 73:232–238
20. Tang ZF, Cheng GJ, Chen YS, Yu XH, Wang HL (2014) Characteristics evaluation of calcium carbonate particles modified by surface functionalization. *Adv Powder Technol* 25:1618–1623

21. Dai YT, Qiu FX, Wang LL, Zhao JL, Yu ZP, Yang P, Yang DY, Kong LY (2014) UV-curable electromagnetic shielding composite films produced through waterborne polyurethane-acrylate bonded graphene oxide: preparation and effect of different diluents on the properties. *E Polym* 14:427–440
22. Hwang HD, Kim HJ (2011) Enhanced thermal and surface properties of waterborne UV-curable polycarbonate-based polyurethane (meth) acrylate dispersion by incorporation of polydimethylsiloxane. *React Funct Polym* 71:655–665
23. Liu BJ, Zhang MY, Liu Y, Tan ZY, Zhou C, Zhang HX (2015) Particle nucleation and growth in the emulsion polymerization of styrene: effect of monomer/water ratio and electrolyte concentration. *J Macromol Sci A* 52:147–154
24. Lee K, Jung H, Kim SY, Lee BH, Choe S (2006) Synthesis and characterization of cross-type vinylurethane macromonomer (C-VUM) and their application in the dispersion polymerization of styrene. *Polymer* 47:1830–1836
25. Yong Q, Pang H, Liao B, Mo W, Huang F, Huang H, Zhao Y (2018) Preparation and characterization of low gloss aqueous coating via forming self-roughed surface based on waterborne polyurethane acrylate hybrid emulsion. *Prog Org Coat* 115:18–26
26. Levine F, La Scala J, Kosik W (2010) Properties of clear polyurethane films modified with a fluoropolymer emulsion. *Prog Org Coat* 69:63–72
27. Wu DM, Qiu FX, Xu HP, Yang DY (2011) Waterborne polyurethane/inorganic hybrid composites: preparation, morphology and properties. *Plast Rubber Compos* 40:449–456
28. Gao XY, Zhu YC, Zhou S, Gao W, Wang ZC, Zhou B (2011) Preparation and characterization of well-dispersed waterborne polyurethane/CaCO₃ nanocomposites. *Colloid Surf A* 377:312–317
29. Guo HX, Qin ZP, Qian P, Yu P, Cui SP, Wang W (2011) Crystallization of aragonite CaCO₃ with complex structures. *Adv Powder Technol* 22:777–783
30. Qiu FX, Xu HP, Wang YY, Xu JC, Yang DY (2012) Preparation, characterization and properties of UV-curable waterborne polyurethane acrylate/SiO₂ coating. *J Coat Technol Res* 9:503–514